Available online at www.sciencedirect.com
SCIENCE DIRECT®
Journal of Organometallic Chemistry 689 (2004) 3685–3700
Journal of Organometallic Chemistry
www.elsevier.com/locate/jorganchem

Selective hydroalkoxycarbonylation of enamides to *N*-acyl amino acid esters: synthetic applications and theoretical studies

S. Klaus [a], H. Neumann [a], H. Jiao [a], A. Jacobi von Wangelin [a], D. Gördes [a], D. Strübing [a], S. Hübner [a], M. Hateley [b], C. Weckbecker [b], K. Huthmacher [b], T. Riermeier [c], M. Beller [a,*]

[a] *Leibniz-Institut für Organische Katalyse an der Universität Rostock e.V. Buchbinderstr. 5-6, 18055 Rostock, Germany*
[b] *Degussa AG, Feed Additives, Hanau, Germany*
[c] *Degussa AG, Degussa Homogeneous Catalysts, Hanau, Germany*

Received 27 April 2004; accepted 2 July 2004
Available online 13 August 2004

Abstract

N-acyl amino acid esters are easily accessible from enamides by cobalt-catalyzed hydroalkoxycarbonylation in moderate to excellent yield. An important reaction parameter for selective carbonylation is the use of low hydrogen partial pressure, which prevents hydrogenation as a side reaction. The reported method is applicable to various enamides and alcohols. A DFT calculation of the catalytic cycle explains the preferred pathway of this reaction.

Keywords: Enamides; Hydroalkoxycarbonylation; Hydroesterification; Homogeneous catalysis; Cobalt; Amino acids; DFT calculations

1. Introduction

The cobalt-catalyzed amidocarbonylation discovered by Wakamatsu et al. [1] is an interesting tool for the synthesis of *N*-acyl amino acids from amides and aldehydes [2]. Although several groups have continuously reported improved catalyst systems [3], as well as employment of various aldehyde analogues or precursors, e.g., olefins [4], oxiranes [5], allylic alcohols [6], and benzyl chloride [7] the method seems to be still somewhat underrated. Apart from cobalt, palladium- [8], and platinum-catalyzed [9] variants of the reaction were investigated more recently. In general, palladium catalysts have the advantage that they work under milder conditions and allow for a larger functional group tolerance [2a]. Nevertheless, cobalt catalysts offer potential advantages because of the significantly lower price of cobalt compared to palladium or platinum. In order to improve the known cobalt-catalyzed amidocarbonylation we decided to study the alkoxycarbonylation of enamides in detail. This strategy eliminates the problems encountered with the different equilibria between aldehydes and amides [10]. The utilization of enamides, which most likely occur as intermediates in the amidocarbonylation cycle, exhibits the additional benefit, that a variety of the corresponding esters are available by utilization of alcohols instead of water. To the best of our knowledge there exists no general cobalt-catalyzed alkoxycarbonylation procedure for enamides and the known catalysts (cobalt, iron, and palladium) deliver the products often in moderate yield [11].

* Corresponding author. Tel.: +49 381 466930; fax: +49 381 4669324.
E-mail address: matthias.beller@ifok.uni-rostock.de (M. Beller).

0022-328X/$ - see front matter © 2004 Elsevier B.V. All rights reserved.
doi:10.1016/j.jorganchem.2004.07.008

2. Results and discussion

2.1. Catalysis

First amidocarbonylation experiments were carried out with the substrate *N*-styrene benzamide, which is a nicely stable enamide and seemed to be a suitable model system for steric and electronic reasons. In addition, the resulting *N*-acyl phenylalanine ester is of some commercial interest for the fine chemical industry. Selected results of this study are shown in Table 1.

In order to activate the applied pre-catalyst $Co_2(CO)_8$ to the "real" catalyst species $HCo(CO)_4$ addition of hydrogen proved to be crucial. Thus, in general a mixture of CO/H_2 was used for the carbonylation experiments. To our surprise already at comparably low CO pressure (40 bar CO) full conversion and a good yield (75%) of *N*-benzoyl phenylalanine methyl ester is obtained (Table 1, entry 1). Here, the main side reaction was hydrogenation of the enamide to give the corresponding alkane. Thus, the influence of the hydrogen partial pressure was investigated in more detail (Table 1, entries 2–7). Lowering the reaction temperature to 100 °C and decreasing the H_2 partial pressure to 2.5 bar still led to an active catalyst, but prevented hydrogenation as side reaction and raised the yield of the desired product to an excellent yield of 97% (Table 1, entry 7).

Interestingly, the addition of phosphine ligands (dppp, NAPHOS, P(*o*-Tol)$_3$, PPh_3, P(*n*-Bu)$_3$; ligand/Co = 2:1) showed a drastic inhibiting influence on the reaction, and almost no conversion was observed. When an excess of CD_3OD was used in the reaction with *N*-styrene benzamide complete replacement of all hydrogens of the former double bond is observed (Scheme 1). Apparently, insertion of the enamide into the Co–D (resulting from the reaction of the acylcobalt-complex with CD_3OD) is a fast and reversible process under the reaction conditions. Thus, exchange of H for D occurs through an olefin insertion-β-hydride elimination sequence.

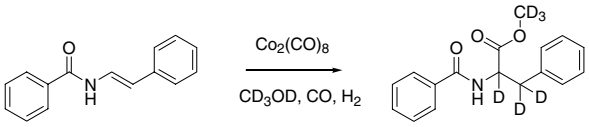

Scheme 1. Hydroalkoxycarbonylation of *N*-styrene benzamide with CD_3OD.

Next, the optimized conditions were applied to various substrates, which differ either in the amide or in the aldehyde moiety of the enamide (Table 2). As shown in Table 2, both the acyl group and the substituents on the enamide double bond significantly influence the reaction. In general, the *N*-benzoyl enamides afforded the corresponding ester in much better yield compared to the corresponding *N*-acetyl derivatives (Table 2, entries 7 vs. 6 and 8 vs. 5). To the best of our knowledge such an influence of the amide group on the carbonylation of enamides has not been reported before. In addition, we also observe an influence of the substitution of the enamide double bond on the yield of the carbonylation products. Here, the unsubstituted vinyl derivative (Table 2, entries 2–4) react best, followed by β-monosubstituted and β,β-disubstituted enamides. Unfortunately, in case of the tetrasubstituted double bond (Table 2, entry 10) no conversion is observed. Apart from methanol, *iso*-propanol and benzyl alcohol react with similar efficiency. It is interesting to note that enamines (and also imines) do not react in the desired manner. Instead hydrogenation occurs as the main reaction here (Table 2, entry 11).

Table 1
Hydroalkoxycarbonylation of *N*-styrene benzamide

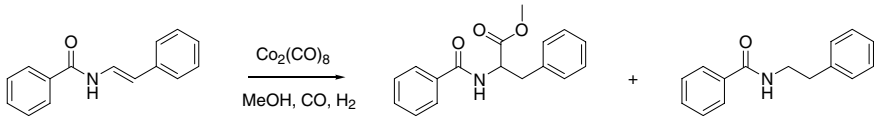

1 **2** **3**

Entry	$Co_2(CO)_8$ (mol%)	MeOH (eq.)	CO/H_2 (bar)	*T* (°C)	Conversion **1** (%) GC	Yield **2** (%) GC	Yield **3** (%) GC
1	2	25	40/10	120	100	75	23
2	2	25	45/5	120	100	84	13
3	2	1.5	45/5	120	54	3	39
4	2	25	45/5	100	98	95	2
5	1	25	45/5	100	85	73	4
6	2	25	47.5/2.5	100	100	95	0
7	2	50	47.5/2.5	100	100	97	0

Reaction conditions: 100-ml autoclave, 500 rpm, 2.5 mmol *N*-styrene benzamide, 25 ml THF, 16 h.

Table 2
Scope and limitation of the cobalt-catalyzed hydroalkoxycarbonylation

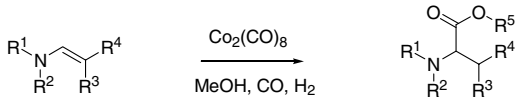

1 2

Entry	Enamide	R^5OH	Conversion **1** (%) GC	Yield **2** [%] (isol.)
1[a]		MeOH	100	59 (51)
2[a]	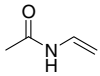	MeOH	100	46 (42)
3[a]		*i*-PrOH	100	51 (47)
4[a]		BnOH	100	57 (55)
5[b]	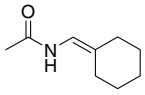	MeOH	100	32 (29)
6[b]	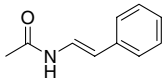	MeOH	100	34 (30)
7[b]	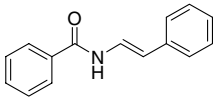	MeOH	100	97 (91)
8[b]	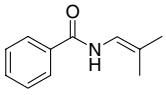	MeOH	100	95 (90)
9[b]	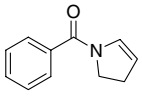	MeOH	100	70 (62)
10[b]	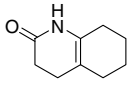	MeOH	0	0
11[b]	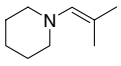	MeOH	57	0
12[b]	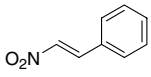	MeOH	0	0
13[b]	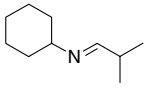	MeOH	15	0

Reaction conditions: 100-ml autoclave, 500 rpm, 2 mol% $Co_2(CO)_8$, 50 eq. alcohol, 47.5/2.5 bar CO/H_2, 10 ml $mmol^{-1}$ THF, 100 °C, 16 h.
[a] 5 mmol educt.
[b] 2.5 mmol educt.

2.2. Theoretical studies

The originally proposed mechanism for the amidocarbonylation reaction considers cobalt tetracarbonyl hydride as a strong acid, which forms with a hemiamidal (resulting from the condensation of amide and aldehyde) an 1-amidoalkylcobalt carbonyl-complex by nucleophilic substitution. After insertion of CO, the resulting cobalt acyl-complex is cleaved exclusively by hydrolysis and no aldehyde is formed, which is in sharp contrast

to olefin hydroformylation. Consequently, it was postulated that water remains ligand-like bound to the cobalt center and cleaves the final acyl complex immediately. Ojima and Zhang [3c] demonstrated that the coordination of the amide oxygen to the acyl cobalt species is necessary for the unique hydrolysis pathway.

These mechanistic models and theories seem to fit only partially to our observations and conditions. Though, we were using enamides, and alcohols as starting materials we tried to find explanations for the different reaction pathways on the basis of computational models and methods. Especially, the nucleophilic addition of a tetracarbonyl cobalt ion seems to be in disaccord with the widely accepted mechanism for the cobalt-catalyzed hydroformylation of olefins [12], which describes a tricarbonyl cobalt hydride as the active catalyst, followed by its coordination to a double bond. In Scheme 2 the different pathways for the reaction of enamides, alcohols and CO/H_2 are shown. Apart from hydroalkoxycarbonylation, in principle hydrogenation and hydroformylation might occur. Especially, the simple hydrogenation was neglected in the existing literature. Consequently, the following investigations deal with the whole catalytic cycle and the practical application of the reaction.

For the cobalt-catalyzed hydroalkoxycarbonylation of enamides to *N*-acyl amino acid esters as described above, we followed the Heck and Breslow [12] mechanism for Co-based hydroformylation reaction in six elementary steps after the generation of the active catalyst: (i) olefin coordination; (ii) olefin insertion; (iii) CO addition; (iv) CO insertion; (v) H_2 oxidative addition; (vi) aldehyde reductive elimination with catalyst regeneration. The structure and bonding of the active catalyst, $HCo(CO)_3$, has been investigated extensively at various levels of theory. A recent work reveals that the planar $HCo(CO)_3$ structure is the most stable singlet state. The loss of an equatorial CO from the precatalyst $HCo(CO)_4$ is the only energetically favored pathway, and other higher energetic alternatives are not competitive [13].

Recently, also the full cycle of propene hydroformylation catalyzed by $HCo(CO)_3$ has been investigated at

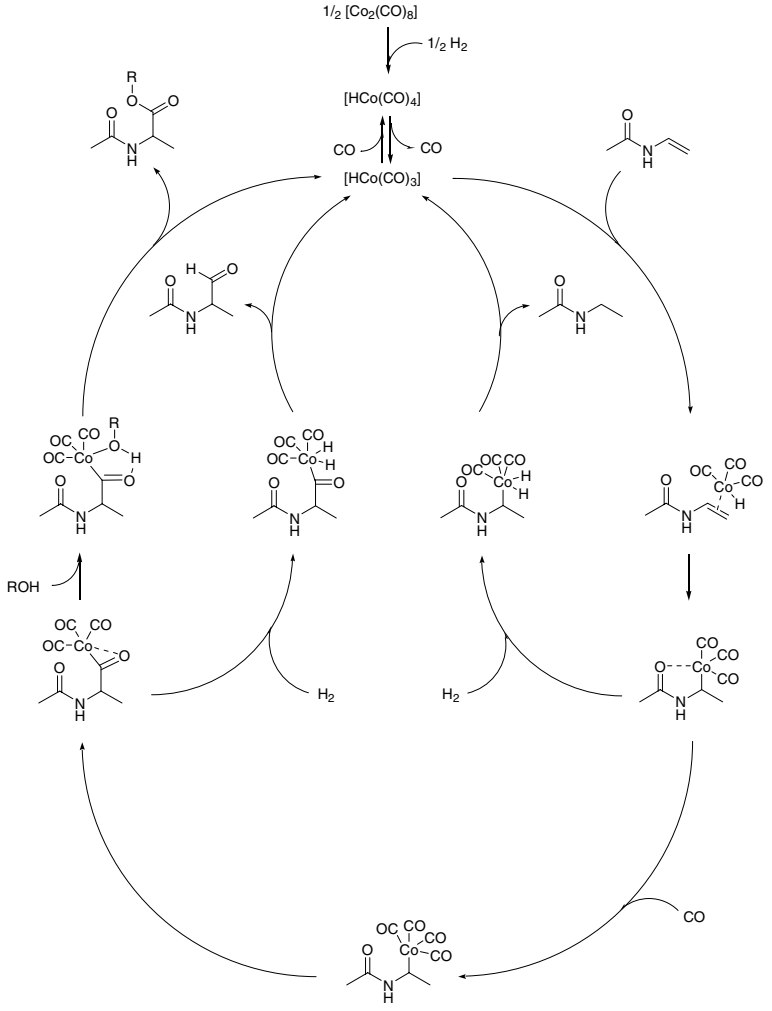

Scheme 2. Competing reaction pathways for hydroalkoxycarbonylation, hydrogenation, and hydroformylation of enamides.

the density functional level of theory [14]. It was found that the regioselectivity is determined by the thermodynamic stability of the alkyl cobalt tetracarbonyl complex ($RCo(CO)_4$) from the exothermic and irreversible CO addition on the alkyl cobalt tricarbonyl complex ($RCo(CO)_3$ + CO). The corresponding process of olefin insertion for the formation of the alkyl cobalt tricarbonyl complex ($RCo(CO)_3$) is reversible, and this explains the observed C=C double bond shift from internal to terminal olefins and vice versa. Here, the rate-determining step is the coordination of H_2 to the acyl cobalt tricarbonyl complex ($RCOCo(CO)_3$).

In this work, we used *N*-vinyl acetamide ($CH_3CONHCH{=}CH_2$) to model enamides. In addition to the oxidative addition of H_2 to the acylcobalt-complex leading to the corresponding aldehyde, nucleophilic substitution by the alcohol (ROH) forms the corresponding *N*-acyl amino acid ester. The hydrogenation of the C=C double bond leading to *N*-ethyl acetamide ($CH_3CONHCH_2CH_3$) was also studied [15]. In principle the alkoxycarbonylation has a similar reaction mechanism to hydroformylation, and both reactions differ only in the step of oxidative addition by using H_2 or methanol. As hydroformylation, hydrogenation has also the same elementary steps of olefin addition and insertion, but they differ in the subsequent step by further coordination of CO or H_2. The calculated free energy profile for the hydroformylation to form aldehyde, for the hydroalkoxycarbonylation to form ester, and for the hydrogenation to form alkane is shown in Scheme 3. Due to their similarity, only the profile for the branched aldehyde and ester is given.

2.2.1. *N*-vinyl acetamide coordination

On the basis of the structural properties of *N*-vinyl acetamide as a substrate, there are four possible coordination modes with the planar $HCo(CO)_3$ as the active catalyst i.e., (i) C=C double bond; (ii) nitrogen lone-pair; (iii) O=C end-on; (iv) O=C side-on. In previous studies [16], we have found that O=C side-on coordination via the oxygen lone-pair is higher in energy than the end-on form via the π-bond by 5.9 kcal/mol, and therefore we did not pay more attention to the O=C side-on coordination.

As found for the propene coordination [14], the propene fragment in the complex can rotate freely because of the small energy barrier, and the most favored conformation is the C=C bond perpendicular to the H–Co axis. The two most favored isomers regarding the methyl substituent *cis* or *trans* to the H–Co bond are isoenergetic. Similarly, there are also rotation isomers for the *N*-vinyl acetamide complex, and the two most stable rotational isomers are very close in energy (<0.1 kcal/mol) and only one isomer is therefore used for discussion. The relative free energies and optimized structures of the *N*-vinyl acetamide complexes are shown in Fig. 1.

For the C=C coordination mode (**1-CC**), Co–C and C=C bond lengths are 2.167/2.307 and 1.392 Å, and they are very close to those in the propene complex. The C=C bond length in **1-CC** is also longer than in the free form (1.348 Å), and this elongation can be

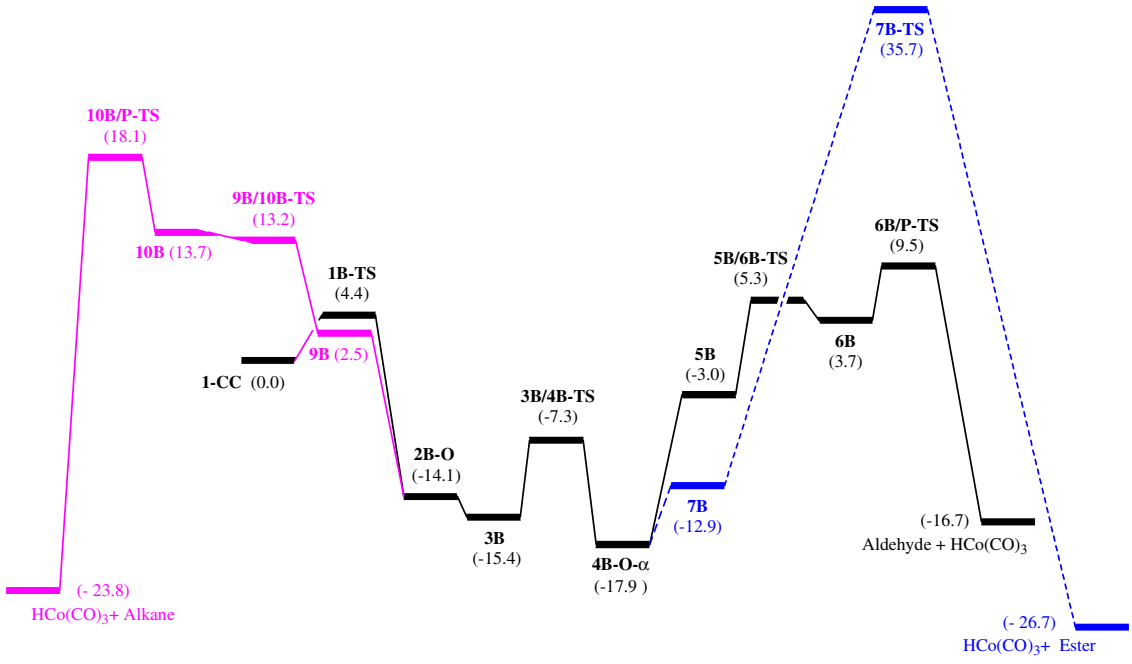

Scheme 3. Computed free energy profile (kcal/mol) for the hydroformylation (solid line), hydroalkoxycarbonylation (dotted blue line) and hydrogenation (solid purple).

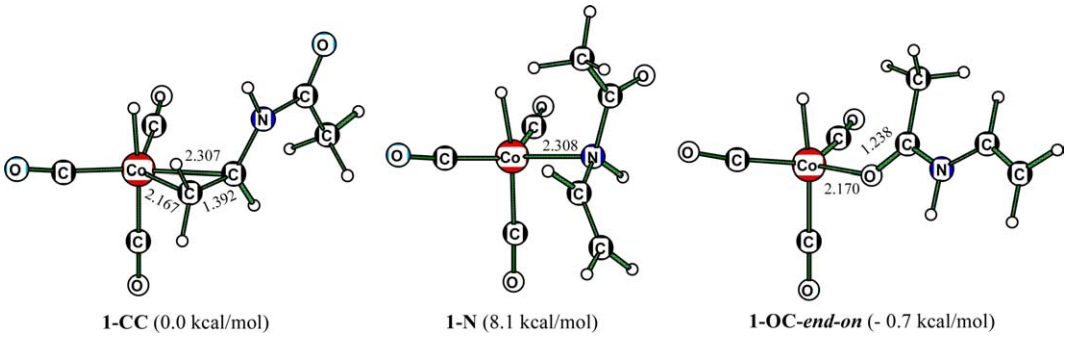

1-CC (0.0 kcal/mol) **1-N** (8.1 kcal/mol) **1-OC-*end-on*** (- 0.7 kcal/mol)

Fig. 1. Optimized bond lengths (Å) and relative free energies (ΔG).

explained by the donation and back donation interaction model of the frontier molecular orbital [17]. In addition, the Co–N bond length in **1-N** is 2.308 Å, and the Co–O distance in **1-OC-*end-on*** is 2.170 Å. It is interesting to note that the most stable coordination mode is **1-OC-*end-on***, and **1-CC** is only 0.7 kcal/mol higher in free energy (**1-CC** is more stable than **1-OC-*end-on*** in enthalpy by 1.7 kcal/mol, respectively). In contrast, **1-N** is the least stable isomer, and 8.8 kcal/mol higher in free energy than **1-OC-*end-on***. These energetic differences indicate that both **1-OC-*end-on*** and **1-CC** can co-exist under an equilibrium in an approximate ratio of 3:1, while the **1-N** form is unlikely. On the basis of these energetic differences and the expected products (Scheme 1), we only used **1-CC** as the starting complex for the further investigations.

2.2.2. Olefin insertion

The insertion of terminal olefins into the Co–H bond can lead to linear and branched alkyl complexes $RCo(CO)_3$ (**L** and **B** notations are used in the text). The linear alkyl complex can be considered as the *anti*-Markovnikow addition product, while the branched complex is the Markovnikov addition product. For olefin insertion, it is necessary to rotate the C═C double bond into the parallel orientation to the H–Co bond, which can facilitate the insertion.

The structures of the two authentic transition states, **1L-TS** and **1B-TS**, are located, and their imaginary vibration modes (624i and 674i cm^{-1}) indicate the migratory insertion of hydrogen to the C═C double bond with the shortening of the H···C distances (1.600 and 1.663 Å) (Fig. 2). Like **1-CC**, the skeleton of **1L-TS** and **1B-TS** around the cobalt center has a distorted trigonal bipyramidal conformation, and the H–Co–C═C torsion angles in **1L-TS** and **1B-TS** are 7.8° and 16.9°. Taking **1-CC** as the starting point, the computed activation free energies for both pathways are 4.3 and 4.4 kcal/mol, respectively. There is therefore no kinetic control over the regioselectivity, and this is in agreement with the findings for the olefin insertion process of the propene complex [14].

As shown in Fig. 2, there are three possible products for the olefin insertion for each individual pathway due to the available functional groups. For example, not only the Co···H–C agostic interaction but also those of the neighboring functional groups (N–H and O═C) at the formally vacant equatorial site of the cobalt center can stabilize the intermediates. It is interesting to note that the three intermediates with branched a alkyl group are energetically more stable than the corresponding isomers with linear alkyl groups. In both cases, the Co···O═C stabilized intermediates are more stable than those stabilized by Co···NH and Co···H–C agostic interactions. For example, **2L-O** is more stable than **2L-N** and **2L-H** by 8.3 and 7.1 kcal/mol, and **2B-O** is more stable than **2B-N** and **2B-H** by 2.1 and 8.2 kcal/mol, respectively. The most interesting point is the free energy difference between **2L-O** and **2B-O**, which is 3.3 kcal/mol. Considering a possible equilibrium between **2B-O** and **2L-O** at 298 K, the predicted distribution ratio for **2B-O**:**2L-O** is 261:1 (or 99.6% for **2B-O**)! Based on these calculations and also on the fact that there is no difference in activation free energy in the insertion process, the formation of **2L-O** is unlikely, and **2B-O** is the sole insertion product. The consequence is that the regioselectivity with *N*-vinyl acetamide as the substrate in hydroformylation and carboxylation is determined by the stability of the branched alkyl product (**2B-O**). This agrees perfectly with the experimental findings shown above.

2.2.3. CO addition and insertion

The subsequent step is the CO addition to the coordinatively unsaturated intermediate $RCo(CO)_3$ (**2L-O/2B-O**) to produce the saturated species $RCo(CO)_4$ (**3L/3B**), followed by the insertion (carbonylation) process leading to the corresponding acyl complexes $(RCO)Co(CO)_3$ (**4L/4B**). The optimized structures and relative energies (relative to **1-CC** and CO) for these species are displayed in Fig. 3.

Structures **3L/3B** represent the most stable conformation of linear and branched cobalt alkyl tetracarbonyl intermediates with the alkyl groups at the axial position,

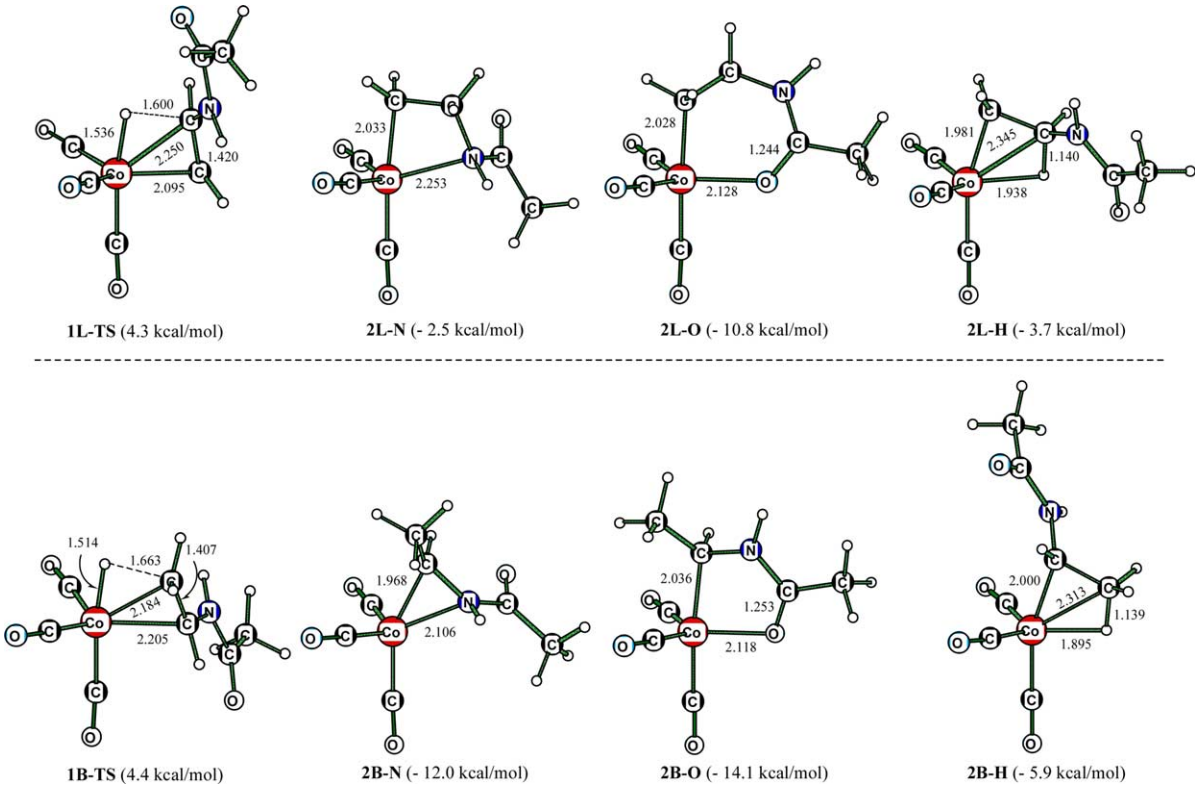

Fig. 2. Optimized bond lengths (Å) and relative free energies (ΔG).

and their free energy difference is 0.8 kcal/mol, which is not only smaller than that (2.1 kcal/mol) between the propyl and isopropyl complexes [14], but also in a revised order. In previous studies, the coordination processes of CO have been computed and the corresponding activation barriers for methyl [18] and (iso)propyl [14] complexes are very small (no barrier for vinyl complex [19]), and the formation of cobalt alkyl tetracarbonyl complexes was found to be highly exergonic. As shown in Fig. 3, the formation of **3L/3B** is also exergonic, and the corresponding energy barrier should be low. Thus, we did not pay any attention to the transition states of CO coordination.

The next step is the CO insertion process from the alkyl complexes **3L/3B** to the acyl complexes **4L/4B**. As in the case of **2L/2B**, there are also three isomers for **4L/4B**, in which the formal vacant coordination position interacts with the neighboring functional group, as shown in Fig. 3. That the fourth possibility with Co···H–C agostic interaction is not considered is because of its rather weak stabilizing effect, as found in **2L-H/2B-H** compared to **2L-O/2B-O** (Fig. 2). In **4L/4B**, all conformations of the acyl species have the acyl group in the axial position. The first intermediate isomer is the η^2-coordination of the acyl group at the α position (**4L-O-α/4B-O-α**). The second one is the end-on coordination of the acyl group from amide (**4L-O/4B-O**). The third alternative is the lone-pair coordination of the amide nitrogen (**4L-N/4B-N**). Apart from **4L-O-α/4B-O-α** with three-membered rings, **4L-O** and **4L-N** have seven- and five-membered rings, while **4B-O** and **4B-N** have six- and four-membered rings due to the different length of the acyl chain, respectively. However, the most stable acyl complexes are (**4L-O-α/4B-O-α**).

In addition to the adducts and products, we have also investigated the corresponding transition states. This process is well studied at various levels of theory. Recent DFT studies showed that the carbonyl insertion reaction proceeds in two steps [14,16,18]. The first step is the migration of the alkyl group to one of the *cis* carbonyl ligands, coupled with the skeletal change from a trigonal bipyramid to a distorted square pyramid with the formation of a three-member ring in the transition state, and then to a butterfly conformation. The second step is the transformation between the different conformers of $(RCO)Co(CO)_3$. Indeed, we have located the authentic transition states on the potential energy surface (**3L/4L-TS** and **3B/4B-TS**) and their negative vibration modes (219i and 119i cm^{-1}) indicate the right direction of the carbonylation. The computed carbonylation barriers for both the linear (**3L** → (**3L/4L-TS**) → **4L**) and the branched routes (**3B** → (**3B/4B-TS**) → **4B**) of 8.7 and 8.1 kcal/mol are comparable, and they are close to those of corresponding step in propene hydroformylation.

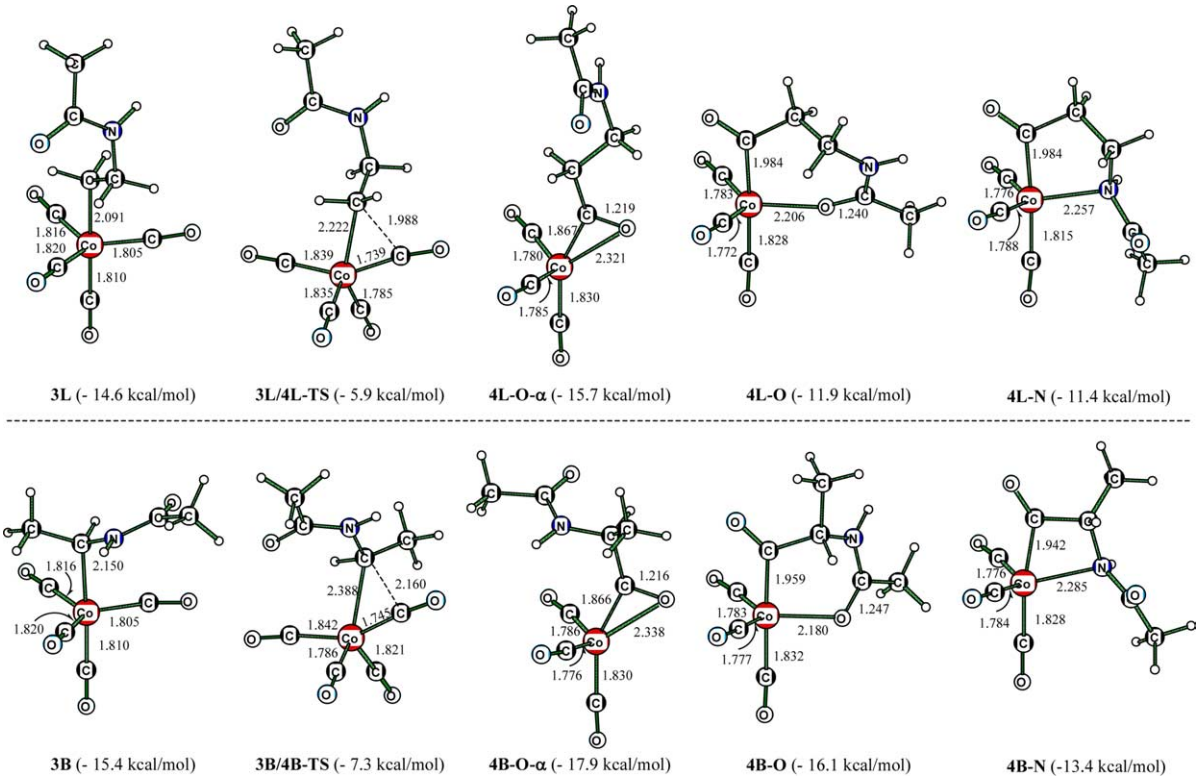

Fig. 3. Optimized bond lengths (Å) and relative free energies (ΔG).

(1) H_2 oxidative addition and aldehyde reductive elimination. The starting point of this step are the most stable isomers from the carbonylation (**4L-O-α/4B-O-α**), and oxidative addition of H_2 leads to the formation of the corresponding aldehydes. The corresponding reaction with CH_3OH leading to the formation of the *N*-acyl amino acid methyl ester is discussed in the following section. The optimized structures and the relative free energies (**1-CC** + CO + H_2) are shown in Fig. 4. In our previous studies [14,16,19], we have found that the coordination of H_2 leading to the formation of the hydrogen adduct is endergonic, and the corresponding transition states have nearly the same energies as the adducts. On this basis and on their similarities in structures and energies, we only payed attention to the hydrogen adducts (**5L/5B**) rather than to their corresponding transition states. As shown in Fig. 4, the H_2 addition complexes (**5L/5B**) are accessible from the η^2-O═C stabilized **4L-O-α/4B-O-α**. In **5L/5B**, H_2 occupies the equatorial site and the H–H bond lies in the basal plane in η^2 coordination. Next, we studied the dihydride complexes (**6L/6B**) and the paths of the oxidative addition reaction. The authentic transition states for the oxidative addition (**5L/6L-TS** and **5B/6B-TS**) have been located on the potential energy surface and the calculated imaginary vibration modes (833i and 879i cm^{-1}) indicate the stretching of the coordinated H–H bond. As shown in Fig. 4, **6L/6B** have the six-coordinated octahedral conformation. Compared with **5L/5B** (0.782/0.783 Å), the H–H distances in **6L/6B** are elongated to 1.836/1.855 Å, accompanying the shortening of the Co–H bonds, respectively. It is interesting to note that in **5L/5B**, the acyl O═C group stands *cis* to the H_2 fragment and bisects the H–H bond, while it rotates away in **6L/6B**, in which the O═C group stands *trans* to one of the Co–H bond, and perpendicular to another Co–H.

For example, the H–Co–C═O torsion angles are 176.4° and 106.3° in **6L**, while 174.5° and 96.4° in **6B**. This perpendicular orientation caused from the simultaneous rotation of the acyl group during the oxidative addition facilitates the subsequent reductive elimination, as indicated in the transition states **6L/P-TS** and **6B/P-TS**, which have the imaginary vibration modes (595i and 562 cm^{-1}) leading to the formation of aldehydes as final products.

On the basis of the most stable acyl complexes, **4L-O-α/4B-O-α**, the H_2 coordination with the formation of **5L/5B** is an endergonic process by 12.6 and 14.0 kcal/mol. The subsequent oxidative addition from **5L/5B** to **6L/6B** is also endergonic by 7.1 and 6.7 kcal/mol, and the corresponding activation free energies are 11.0 and 8.3 kcal/mol, respectively. The next step is the reductive elimination from **6L/6B** to the products (aldehyde) and the active catalyst, and this process is exergonic, and the corresponding activation free energies are 2.9 and 5.8 kcal/mol, respectively. Due to the available

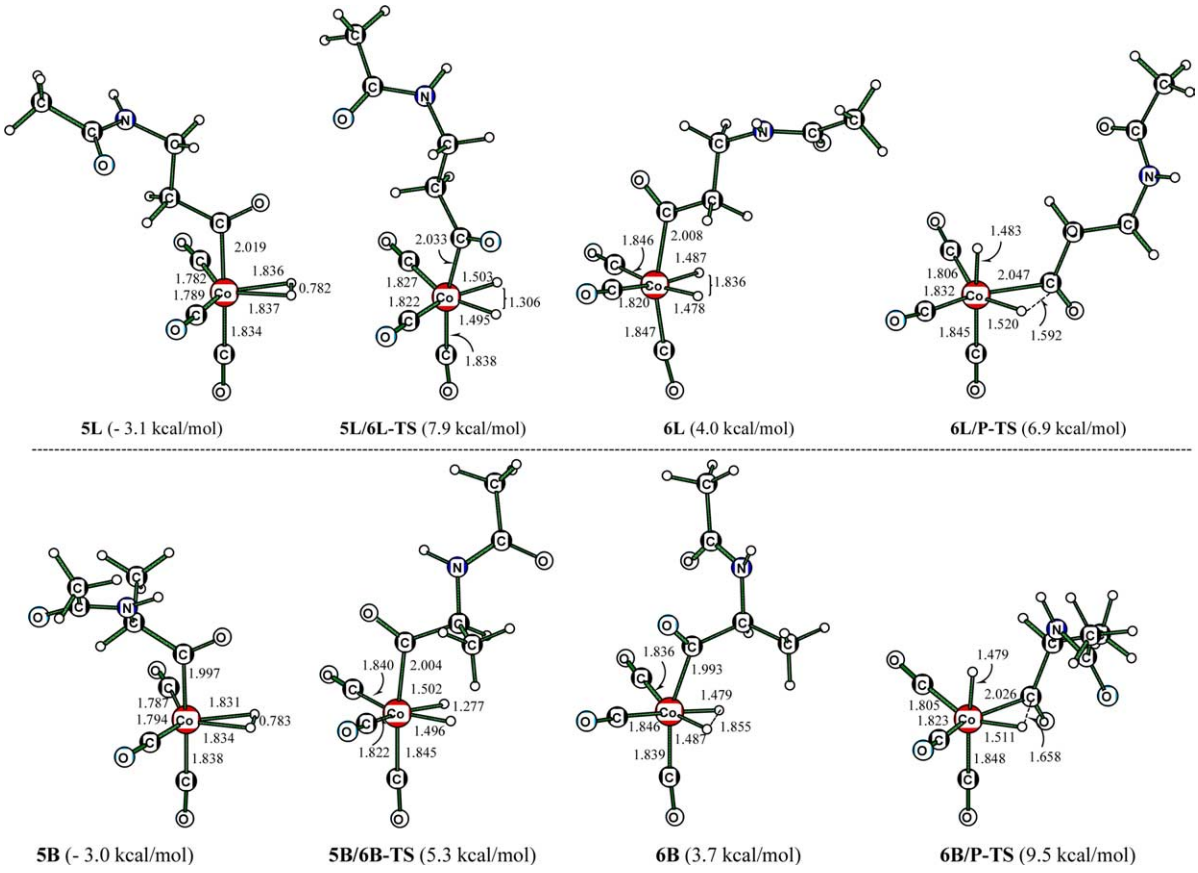

Fig. 4. Optimized bond lengths (Å) and relative free energies (ΔG).

functional groups in the formed aldehydes, we used the separated $HCo(CO)_3$ and aldehyde to calculate the changes of free energies, and this will simplify the complicated analysis of the possible intermediates between $HCo(CO)_3$ and the aldehyde. Taking **1-CC** and ($CO + H_2$) as the starting point, the formation of the linear and branched product is exergonic by 15.4 and 16.7 kcal/mol, respectively.

(2) Carboxylation of N-vinyl acetamide ($CH_3CONHCH{=}CH_2$). Since the main goal of our experimental investigation is the carboxylation of enamides to *N*-acyl amino acid esters, we have also studied the corresponding elementary step for the formation of the ester, e.g., the reaction with CH_3OH instead of H_2 and the reductive elimination of ester instead of aldehyde. Clearly, both hydroformylation and carboxylation have the same elementary steps in olefin addition and insertion, and the subsequent carbonylation. The optimized structures and relative free energies (related to **1-CC** + CO + CH_3OH) are given in Fig. 5. As in the case of H_2 coordination, we have also located two methanol adducts **7L/7B**. However, it is interesting to note that the H–O bonds in **7L/7B** are parallel to the Co–C_{acyl} bonds, while the H–H bond in **5L/5B** are perpendicular to the Co–C_{acyl} bonds. One reason for this conformation in **7L/7B** is the attractive electrostatic interaction between the polar H–O bond and the acyl C═O bond. The H···O distances in **7L/7B** are 1.741 and 1.749 Å, respectively, and the formal H–O–Co–C═O five-membered rings are nearly planar. For the oxidative addition, we have located the corresponding transition state, **7L-TS/7B-TS**, but many attempts to locate the corresponding intermediates (the hydride and methoxo complex) from the oxidative addition failed and further optimization following the negative vibration modes lead to the formation of the final products directly without any barrier. This indicates that the potential energy surface is flat. The driving force for the simplified reaction might be the attractive electrostatic interaction between the negatively charged oxygen center of the CH_3O ligand and the positively charged carbon center of the acyl ligand, both ligands already have the appropriate orientation, which can facilitate further reaction.

On the basis of the most stable acyl intermediates (**4L-O-α**and **4B-O-α**), the coordination of CH_3OH is slightly endergonic by 2.7 and 5.0 kcal/mol for **7L** and **7B**. Hence, they are also less endergonic than the H_2 adducts (**5L/5B**, Fig. 4), respectively. However, the

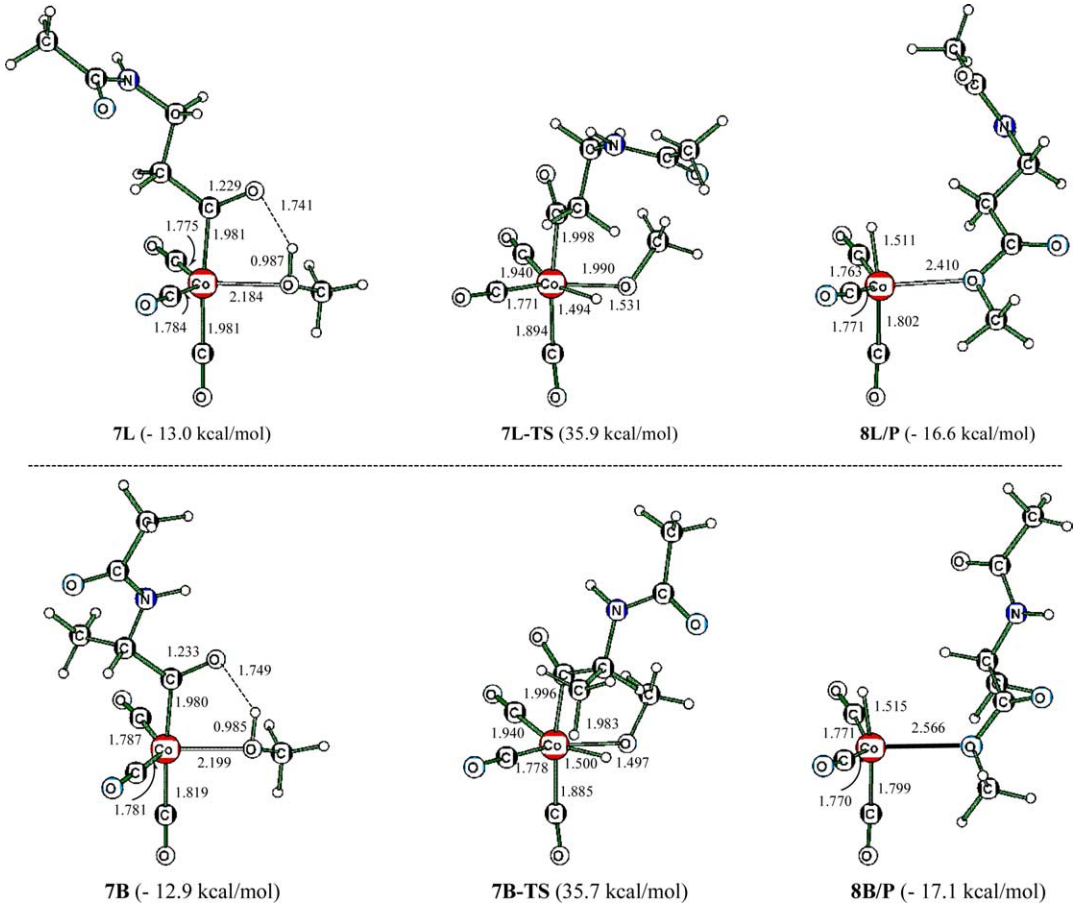

Fig. 5. Optimized bond lengths (Å) and relative free energies (ΔG).

activation free energies for the oxidative addition of the H–OCH_3 bond by 48.9 and 48.6 kcal/mol are very high, and they are comparable to those of the H–N bond oxidative addition (49 kcal/mol [20]), respectively. This activation free energy explains the low yield compared to hydroformylation. Since it is not possible to locate the corresponding intermediates of the oxidative addition, and the subsequent transition states for the reductive elimination, no energetic data for these species are available. From the CH_3OH adducts, the formation of the ester complexes **8L/P** and **8B/P** are slightly exergonic by 3.6 and 4.2 kcal/mol, respectively. Taking **1-CC** and (CO + CH_3OH) as the starting point, the formation of the separated product and $HCo(CO)_3$ are exergonic for the linear and branched esters by 25.5 and 26.7 kcal/mol, respectively.

(3) Hydrogenation of N-vinyl acetamide ($CH_3CONHCH{=}CH_2$). In addition to the hydroformylation and carboxylation of enamide, we also were interested in the corresponding hydrogenation, which is competitive and responsible for the formation of alkanes as by-products. Since both hydroformylation and hydrogenation have the same elementary steps of olefin addition and insertion, we only studied the steps of H_2 oxidative addition and reductive elimination leading to the expected hydrogenated products. Recently, hydrogenation of the C=C bond in acrolein [16], and the C≡C bond in acetylene [19] has been investigated systematically. Since both acrolein and *N*-vinyl amide can be considered as substituted olefins, their catalytic cycles are somewhat similar. Therefore, we discuss the general results briefly and emphasize the differences specifically.

As in the case of alkoxycarbonylation and hydroformylation, the starting point for hydrogenation is the alkylcobalt-complex ($RCo(CO)_3$, **2L-O** and **2B-O** in this work) formed from the olefin insertion step. Then, oxidative addition of H_2 might take place and subsequently reductive elimination forms the alkane in general. The optimized structures and relative free energies (relative to **1-CC** and H_2) are shown in Fig. 6. It should also be noted that reaction free energies and the structural parameters of the H_2 oxidative addition and the reductive elimination for hydrogenation are similar to those found in the step of hydroformylation (Fig. 4).

As shown in Fig. 6, the most stable hydrogen adducts (**9L/9B**) have the H_2 at the equatorial position and the H–H bond is perpendicular to the Co–C_{alkyl} bond.

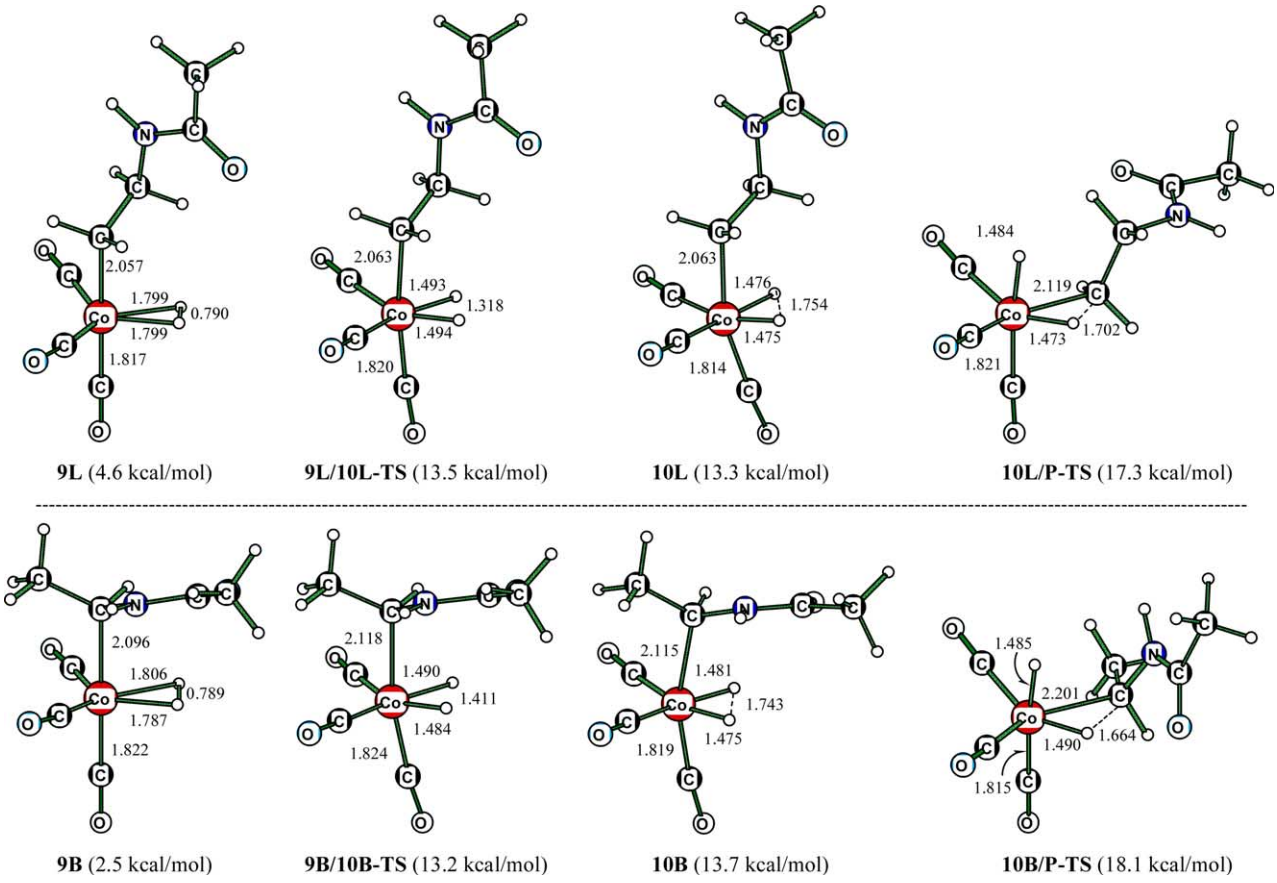

Fig. 6. Optimized bond lengths (Å) and relative free energies (ΔG).

The next step is the formation of the dihydride complexes (**10L/10B**) from the oxidative addition. It is interesting to note that **10L/10B** have distorted octahedral geometries. Compared with the corresponding η^2 complexes **9L/9B**, the main change in **10L/10B** is the dissociation of the H–H bond accompanying the shortening of the Co–H bonds. In addition, it is possible to locate the authentic transition states on the potential energy surface, and the calculated imaginary vibration modes (782i and 522i cm^{-1}) of the transition states (**9L/10L-TS** and **9B/10B-TS**) indicate the breaking of the coordinated H–H bond, and this leads to the formation of the dihydride complexes (**10L/10B**). The reductive elimination from **10L/10B** proceeds by one of the hydride ligands migrating and attacking the first alkyl carbon atom. It is clearly shown that this process goes via the three-center transition state **10L/P-TS** and **10B/P-TS**, and the computed imaginary vibration modes (748i and 699i cm^{-1}) indicate the formation of the C–H bonds.

As illustrated in Fig. 6, the H_2 addition from the most stable alkyl complexes (**2L-O** and **2B-O**) are endergonic by 15.4 and 16.6 kcal/mol, and the computed free activation energies for the oxidative addition leading to the dihydride complexes (**10L/10B**) are 8.9 and 10.7 kcal/mol, respectively. However, the barriers for the reductive elimination of 4.0 and 4.4 kcal/mol are rather small, and the subsequent formation of the separated products and $HCo(CO)_3$ are exergonic by 23.8 kcal/mol. The computed energetic data for the whole reactions are summarized in Table 3.

(4) Coordination of $HCo(CO)_3$ with different amido-, amino-substituted olefins and imines. In addition to the unsubstituted *N*-vinyl acetamide, other amido- and amino-substituted olefins were used in the experimental work. In order to explain the difference in reactivity of these substrates the relative free coordination energies of possible coordination isomers within a given substrate with $HCo(CO)_3$ were calculated. The obtained data are summarized in Table 4.

As discussed above, the most stable complex between $HCo(CO)_3$ and *N*-vinyl acetamide (CH_3CO–NH–CH=CH_2) is **1-OC-*end-on***, followed by **1-CC** by 0.7 kcal/mol. The nitrogen coordination (**1-N**) is much higher in energy by 8.8 kcal/mol. This indicates that **1-OC-*end-on*** and **1-CC** can exist in an approximate equilibrium with a ratio of 3:1, and **1-N** is therefore energetically unlikely. We have also tried to locate the η^2-O=C coordination, but the optimization results

Table 3
B3LYP/LANL2DZp computed total electronic energies (E_{tot}, au), free energies (G_{tot} (298 K), au) and zero-point energies (ZPE, kcal/mol) as well as number of imaginary frequencies (N_{Imag})

Compound	E_{tot}	ZPE (N_{Imag})	G_{tot} (298 K)
Starting materials			
$HCo(CO)_3$	−485.74438	19.4 (0)	−485.74754
H_3 CCO–NHCH=CH_2	−286.64715	67.2 (0)	−286.57069
H_2	−1.17442	6.4 (0)	−1.17575
CH_3 OH	−115.73945	32.2 (0)	−115.71089
CO	−113.32896	3.1 (0)	−113.34313
Olefin coordination and insertion			
1-CC	−772.41100	88.5 (0)	−772.31472
1-OC-end-on	−772.40827	87.9 (0)	−772.31583
1-N	−772.39580	87.9 (0)	−772.30184
1L-TS	−772.40183	87.8 (1)	−772.30782
1B-TS	−772.40147	87.7 (1)	−772.30775
2L-N	−772.41939	91.2 (0)	−772.31866
2L-O	−772.43347	91.5 (0)	−772.33193
2L-H	−772.41779	90.3 (0)	−772.32059
2B-N	−772.43356	90.8 (0)	−772.33388
2B-O	−772.43799	90.9 (0)	−772.33726
2B-H	−772.42211	90.2 (0)	−772.32417
CO insertion (carbonylation)			
3L	−885.78496	96.3 (0)	−885.68105
3B	−885.78623	95.8 (0)	−885.68241
3L/4L-TS	−885.77033	96.0 (1)	−885.66719
3B/4B-TS	−885.77422	95.7 (1)	−885.66956
4L-N	−885.78525	97.7 (0)	−885.67603
4L-O-α	−885.78609	96.9 (0)	−885.68285
4L-O	−885.78482	97.5 (0)	−885.67678
4B-N	−885.78572	96.8 (0)	−885.67922
4B-O-α	−885.79397	97.0 (0)	−885.68644
4B-O	−885.78647	96.5 (0)	−885.68348
H_2 oxidative addition and aldehyde reductive elimination			
5L	−886.95695	106.5 (0)	−886.83849
5L/6L-TS	−886.93876	105.7 (1)	−886.82108
6L	−886.94587	107.0 (0)	−886.82575
6L/P-TS	−886.94142	106.2 (1)	−886.82255
5B	−886.95709	106.3 (0)	−886.83832
5B/6B-TS	−886.94414	105.6 (1)	−886.82518
6B	−886.94839	106.7 (0)	−886.82774
6B/P-TS	−886.93827	105.8 (1)	−886.81846
Carbonylation			
7L	−1001.54373	131.2 (0)	−1001.38949
7L-TS	−1001.45897	126.8 (1)	−1001.31154
8L/P	−1001.54385	129.4 (0)	−1001.39514
7B	−1001.54454	130.9 (0)	−1001.38932
7B-TS	−1001.46009	126.6 (1)	−1001.31178
8B/P	−1001.54483	129.0 (0)	−1001.39593
Olefin hydrogenation			
9L	−773.59653	100.8 (0)	−773.48317
9B	−773.60102	100.5 (0)	−773.48647
9L/10L-TS	−773.58141	100.0 (1)	−773.46893
9B/10B-TS	−773.58272	99.8 (0)	−773.46936
10L	−773.58335	101.2 (0)	−773.46933
10B	−773.58350	100.9 (0)	−773.46865
10L/P-TS	−773.57602	100.5 (1)	−773.46298
10B/P-TS	−773.57514	100.2 (1)	−773.46156

Table 3 (*continued*)

Compound	E_{tot}	ZPE (N_{Imag})	G_{tot} (298 K)
Products from three reaction			
n-aldehyde	−401.21435	87.6 (0)	−401.11073
Iso-aldehyde	−401.21569	87.4 (0)	−401.11274
n-ester	−515.79523	109.0 (0)	−515.66187
Iso-ester	−515.79827	108.8 (0)	−515.66380
$CH_3CONHC_2H_5$	−287.87858	81.9 (0)	−287.78089

Table 4
B3LYP/LANL2DZp total free energies (au) and the relative free energies (kcal/mol, in parentheses) for a set of selected substrates with $HCo(CO)_3$

Substrate	C═C/π	N/LP	O/LP
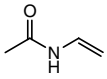	−772.31472 (0.0)	−772.30184 (+8.1)	−772.31583 (−0.7)
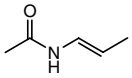	−811.60846 (0.0)	−811.59758 (+6.8)	−811.61305 (−2.9)
	−698.23639 (0.0)	−698.22455 (+7.4)	
	−768.86173 (0.0)	Goes to O/LP	−768.85586 (+3.7)
	−658.94538 (0.0)[a]	−658.96610 (−13.0)	
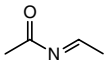	−772.30600 (0.0)[a]	−772.31682 (−6.8)	−772.31564 (−6.1)

[a] C═N coordination.

in **1-OC-*end-on***. The same qualitative results are also found for the β-methyl-substituted enamide CH_3CO–NH–CH═$CHCH_3$.

However, for enamines (R = $N(CH_3)_3$) the C═C double coordination is more favored in free energy than the nitrogen sp^3 lone-pair mode by 7.4 kcal/mol. For the nitro-substituted olefin (R = NO_2) it should be noted that coordination with nitrogen sp^3 lone-pair does not exist on the potential energy surface, and optimization results in the coordination mode with one of the oxygen atoms of the NO_2 group. Nevertheless, the C═C double bond coordination is more stable than the oxygen mode by 3.7 kcal/mol.

Interestingly, for imines such as *trans*-CH_3–CH═N–R, it is found that the nitrogen sp^2 lone-pair coordination is more favored that the corresponding N═C double coordination, e.g., by 13.0 kcal/mol for R = CH_3, and 6.8 kcal/mol for R = CH_3CO. This is in line with the enhanced basicity of the nitrogen sp^2 lone pair compared to the nitrogen sp^3 lone-pair. In addition, we have tried to locate the O═C double bond coordinated isomer for R = CH_3CO, but optimization leads to the only oxygen coordination, which is close in energy with that of the sp^2 lone pair mode.

3. Conclusions

In summary, we have shown that hydroalkoxycarbonylation of different enamides proceeds well in the presence of $Co_2(CO)_8$ as a pre-catalyst with the application of an optimized CO/H_2 ratio. Interestingly, enamides with an *N*-benzoyl group give significantly higher yields compared to *N*-acetyl enamides.

Theoretical investigations demonstrate that the regioselectivity of the alkoxycarbonylation is determined by the relative stability of the alkyl complexes stabilized by the interaction between the neighboring O═C group and the formally vacant coordination position at the cobalt center. The intermediate with a branched alkyl group is more stable than that with a linear alkyl group by 3.3 kcal/mol, and only the final product with a branched alkyl chain can be observed, which explains nicely the experimental findings. In addition, there is no energetic difference in the transition state of olefin insertion, and therefore the observed regioselectivity is controlled thermodynamically.

In contrast to the H_2 oxidative addition in the hydroformylation and hydrogenation reaction pathway, the

alkoxycarbonylation process does not have an oxidative addition intermediate (the hydrido and methoxy complexes) and reductive elimination transition state. The reason for this rather flat potential energy surface is due to the negative charge of the methoxy group and the polar acyl group. Here, the attractive interaction leads directly to the final product. Beside these calculated reaction pathways the nucleophilic addition of methanol was observed in some cases. However, this reaction pathway is reversible under the used conditions. It is also interesting to note that C═C double bond coordination is generally more favored over the coordination of the nitrogen sp^3 lone-pair in $CH_3CO–NH–CH═CHR$, and $H_2C═CH–NHCH_3$ and $H_2C═CH–N(CH_3)_2$. In contrast, the nitrogen sp^2 lone-pair coordination is more favored over the N═C double bond in $CH_3–CH═NR$. This difference is in line with the basicity of nitrogen sp^2 and sp^3 lone-pairs and might explain the not observed reactivity of imines under the applied reaction conditions.

4. Experimental

4.1. General

Enamides, enamines, and imines were synthesized by literature methods. Alcohols and dodecane (internal standard) were purchased by Aldrich in water free quality and were used without further purification. THF was distilled from sodium and benzophenone. $Co_2(CO)_8$ was purchased from Fluka. All isolated products were fully characterized after isolation (^{1}H NMR, $^{13}C\{^1H\}$ NMR, IR, MS, and HRMS).

4.2. General procedure

A inert schlenk reaction flask (50–100 ml) was charged with the corresponding enamide (2.5 or 5 mmol), $Co_2(CO)_8$ (2 mol%), and purged with argon. Then THF (10 ml/mmol), alcohol (50 eq), and dodecane (0.5 eq, internal standard) were added. The homogenous reaction mixture was transferred by a tube into an inert autoclave (100 ml, Parr), which was pressurized afterwards with CO (47.5 bar) and H_2 (2.5 bar). After stirring for 16 h at 100 °C, the autoclave was cooled in a nice bath and the residual gases were removed. Work up of the reaction mixture was performed by flash column chromatography (SiO_2, *n*-heptane/EtOAc).

5. Analytical data

5.1. Methyl 2-(2-oxo-pyrrolidin-1-yl)propionate

Colorless oil; R_f (SiO_2, EtOAc): 0.32; ^{1}H NMR (400 MHz, $CDCl_3$, 297 K): δ = 4.75 (q, J = 7.53 Hz, 1H, NC*H*COO), 3.60 (s, 3H, OCH_3), 3.33 (m, J = 1.98/7.53 Hz, 2H, NCH_2), 2.30 (m, J = 1.98 Hz, CH_2CO), 1.95 (m, 2H, CH_2CH_2N), 1.30 (d, J = 7.53 Hz, 3H, NCHCH_3); $^{13}C\{^1H\}$ NMR (101 MHz, $CDCl_3$, 297 K): δ = 175.0 (*C*O), 171.6 (*C*OO), 51.9 (N*C*HCH$_3$), 48.9 (O*C*H$_3$), 43.2 (*C*H$_2$N), 30.5 (*C*H$_2$CO), 17.8 (*C*H$_2$CH$_2$N), 14.5 (NCH*C*H$_3$); IR (kap/KBr, cm^{-1}): 2954 s, 2766 w, 1744 vs, 1695 vs, 1492 m, 1461 s, 1423 vs, 1378 m, 1355 m, 1288 vs, 1206 vs, 1118 m, 1082 s, 854 m, 636 w; MS (EI): *m*/*z* (%) = 171 $[M]^+$ (7), 112 (100), 84 (14), 69 (29), 56 (11), 41 (19), 28 (11), no other peaks >10%; HRMS Calc. for $C_8H_{13}NO_3$: 171.08954. Found: 171.08844.

5.2. Methyl 2-acetylaminopropionate

Colorless oil; R_f (SiO_2, EtOAc): 0.19; ^{1}H NMR (400 MHz, $CDCl_3$, 297 K): δ = 6.60 (d, J = 6.63 Hz, 1H, N*H*), 4.52 (t*, J = 6.63/7.22 Hz, 1H, NHC*H*), 3.68 (s, 3H, OCH_3), 1.96 (s, 3H, CH_3CO), 1.33 (d, J = 7.22 Hz, 3H, NHCHCH_3); $^{13}C\{^1H\}$ NMR (101 MHz, $CDCl_3$, 297 K): δ = 173.5 (*C*O), 170.1 (*C*OO), 52.3 (O*C*H$_3$), 47.9 (NH*C*H), 22.7 (*C*H$_3$CO), 18.1 (NHCH*C*H$_3$); IR (kap/KBr, cm^{-1}): 3287 s, 3071 m, 2988 m, 2955 m, 2602 vw, 1747 vs, 1657 vs, 1547 vs, 1457 s, 1376 s, 1307 m, 1274 m, 1214 s, 1164 s, 1060 m, 985 w, 850 w, 669 vw, 595 vw; MS (EI): *m*/*z* (%) = 145 $[M]^+$ (2), 86(38), 44 (100), 28 (12), no other peaks >10%; HRMS Calc. for $C_{12}H_{11}NO_3$: 145.07390. Found: 145.07360.

5.3. Isopropyl 2-acetylaminopropionate

Colorless oil; R_f (SiO_2, EtOAc): 0.30; ^{1}H NMR (400 MHz, $CDCl_3$, 297 K): δ = 6.58 (s, 1H, N*H*), 4.93 (d(7), J = 6.23/1.98 Hz, 1H, C*H*(CH$_3$)$_2$), 4.42 (d(5), J = 7.37/1.98 Hz, 1H, NHC*H*), 1.91 (d, J = 1.42 Hz, 3H, CH_3CO), 1.27 (dd*, J = 1.70/7.37 Hz, 3H, NHCHCH_3), 1.15 (dt*, J = 1.70/6.23 Hz, 6H, CH(CH_3)$_2$); $^{13}C\{^1H\}$ NMR (101 MHz, $CDCl_3$, 297 K): δ = 172.5 (*C*O), 169.7 (*C*OO), 68.7 (*C*H(CH$_3$)$_2$), 47.9 (NH*C*H), 22.7 (*C*H$_3$CO), 21.5 and 21.4 (CH(*C*H$_3$)$_2$), 18.0 (NHCH*C*H$_3$); IR (kap/KBr, cm^{-1}): 3290 s, 3070 m, 2983 s, 2939 m, 2880 w, 1740 vs, 1357 vs, 1546 vs, 1456 s, 1376 vs, 1307 s, 1276 s, 1211 vs, 1171 vs, 1109 vs, 1058 m, 932 w, 755 w, 694 w, 594 m, 519 w; MS (EI): *m*/*z* (%) = 173 $[M]^+$ (3), 114 (17), 86 (18), 43 (100), 28 (19), no other peaks >10%; HRMS Calc. for $C_8H_{15}NO_3$: 173.10519. Found: 173.10487.

5.4. Benzyl 2-acetylaminopropionate

Colorless oil; R_f (SiO_2, EtOAc/*n*-heptane 1/1): 0.28; ^{1}H NMR (400 MHz, $CDCl_3$, 297 K): δ = 7.27–7.17 (m, 5H, Ph), 7.00 (s, 1H, N*H*), 5.00 (d, 2H, CH_2Ph), 4.49 (d(5), J = 7.07 Hz, 1H, NHC*H*CH$_3$), 1.88 (s, 3H, CH_3CO), 1.28 (dd, J = 7.07 Hz, 3H, NHCHCH_3);

$^{13}C\{^1H\}$ NMR (101 MHz, $CDCl_3$, 297 K): δ = 172.6 (*C*O), 169.9 (*C*OO), 135.1 (*i-C*), 128.2 (*m-C*H), 127.9 (*p-C*H), 127.6 (*o-C*H), 66.5 (CH_2Ph), 47.8 (NH*C*H), 22.4 and 17.5 (NHCH*C*H_3); IR (KBr, cm^{-1}): 3283 m, 3066 w, 2983 w, 2939 w, 1746 vs, 1660 vs, 1546 s, 1456 s, 1374 m, 1303 m, 1264 m, 1204 s, 1159 vs, 1058 w, 973 vw, 751 m, 699 m, 599 vw; MS (EI): *m/z* (%) = 221 $[M]^+$ (1), 114 (11), 91 (100), 87 (30), 77 (10), 65 (26), 43 (49), 28 (15), no other peaks >10%; HRMS Calc. for $C_{12}H_{15}NO_3$: 221.10519. Found: 221.10447.

5.5. Methyl N-acetyl-2-cyclohexylidenglycinate

Colorless solid; m.p.: 72–74 °C; R_f (SiO_2, EtOAc): 0.39; ^1H NMR (400 MHz, $CDCl_3$, 297 K): δ = 6.13 (d, *J* = 8.52 Hz, 1H, N*H*), 4.51 (dd*, *J* = 5.35/8.52 Hz, 1H, NHC*H*), 3.70 (s, 3H, OCH_3), 2.00 (s, 3H, CH_3CO), 1.77–1.67 (m, 3H, Cy), 1.66–1.54 (m, 3H, Cy), 1.26–1.11 (m, 2H, Cy), 1.10–0.95 (m, 3H, Cy); $^{13}C\{^1H\}$ NMR (101 MHz, $CDCl_3$, 297 K): δ = 172.7 (*C*O), 169.9 (*C*OO), 56.7 and 52.0 (NH*C*H and COO*C*H_3), 40.8 (NHCH*C*H), 29.3, 28.3, 25.9, and 25.8 (Cy), 23.1 (*C*H_3CO); IR (KBr, cm^{-1}): 3264 s, 3066 w, 2927 s, 2855 s, 1747 vs, 1651 vs, 1550 s, 1433 s, 1376 s, 1297 s, 1229 m, 1206 s, 1171m, 1149 s, 986 m, 727 w, 604 w; MS (EI): *m/z* (%) = 214 $[M + H]^+$ (100), 182 (11), 154 (24), no other peaks >10%, HRMS Calc. for $C_{11}H_{19}NO_3$: 213.13649. Found: 213.13692.

5.6. Methyl 2-acetylamino-3-phenylpropionate

Colorless solid; m.p.: 85 °C; R_f (SiO_2, 1:2 *n*-heptane/EtOAc): 0.3; ^1H NMR (400 MHz, $CDCl_3$, 297 K): δ = 7.32–7.22 (m, 3H, Ph), 7.11–7.07 (m, 2H, Ph), 6.03 (d, *J* = 7.85 Hz, 1H, N*H*), 4.89 (dt, *J* = 7.85/5.64 Hz, 1H, NHC*H*), 3.37 (s, 2H, OCH_3), 3.12 (m, 5.64 Hz, 2H, NHCHCH_2), 1.98 (s, 3H, CH_3CO); $^{13}C\{^1H\}$ NMR (101 MHz, $CDCl_3$, 297 K): δ = 172.1 (*C*O), 169.6 (*C*OO), 135.8 (*i-C*), 129.2 (*m-C*H), 128.5 (*o-C*H), 127.1 (*p-C*H), 53.1 and 52.3 (O*C*H_3 and NH*C*H), 37.8 (NHCH*C*H_2), 23.1 (*C*H_3CO); IR (KBr, cm^{-1}): 3336 vs, 3069 vw, 3035 vw, 2962 vw, 2935 vw, 1754 vs, 1650 vs, 1538 s, 1457 m, 1438 m, 1377 m, 1286 m, 1221 s, 1191 s, 1174 s, 1123 m, 1086 w, 977 w, 764 m, 748 m, 707 m, 675 w, 592 w; MS (EI, 70 eV): *m/z* (%) = 221 $[M]^+$ (2), 162 (100), 131 (26), 120 (39), 91 (35), 88 (68), 65 (10), 43 (38), no other peaks >10%; HRMS Calc. for $C_{12}H_{15}NO_3$: 221.10519. Found: 221.10608.

5.7. Methyl 2-benzoylamino-3-phenylpropionate

Colorless solid; m.p.: 75 °C; R_f (SiO_2, EtOAc): 0.7; ^1H NMR (400 MHz, $CDCl_3$, 297 K): δ = 7.67–7.60 (m, 2H, Ph), 7.44–7.37 (m, 1H, Ph), 7.36–7.28 (m, 2H, Ph), 7.24–7.13 (m, 3H, Ph), 7.08–7.02 (m, 2H, Ph), 6.59 (d, *J* = 7.09 Hz, 1H, N*H*), 5.00 (dt, *J* = 5.84/7.09 Hz, 1H, NHC*H*), 3.67 (s, 3H, OCH_3), 3.17 (dq, *J* = 5.84 Hz, 2H, NHCHCH_2); $^{13}C\{^1H\}$ NMR (101 MHz, $CDCl_3$, 297 K): δ = 172.0 (*C*O), 166.8 (*C*OO), 135.8 (*i-C*), 133.8 (*i-C*), 131.7 (*p-C*H), 129.2 (Ph), 128.6 (Ph), 128.5 (Ph), 127.1 (*p-C*H), 126.9 (Ph), 53.5 and 52.3 (O*C*H_3 and NH*C*H), 37.8 (NHCH*C*H_2); IR (KBr, cm^{-1}): 3317 m, 3063 vw, 3030 w, 2950 w, 1756 s, 1740 vs, 1640 vs, 1529 s, 1491 m, 1434 m, 1324 m, 1217 s, 1174 m, 699 s; MS (EI): *m/z* (%) = 283 $[M]^+$ (2), 224 (5), 162 (57), 131 (10), 105 (100), 91 (12), 77 (40), 51 (9), no other peaks >10%; HRMS (ESI) Calc. for $C_{17}H_{18}NO_3$: 284.12866. Found: 284.12327.

5.8. Methyl 2-benzoylamino-3-methylbutyrate

Colorless solid; m.p.: 105–106 °C; R_f (SiO_2, EtOAc): 0.84; ^1H NMR (400 MHz, $CDCl_3$, 297 K): δ = 7.84–7.76 (m, 2H, Ph), 7.54–7.39 (m, 3H, Ph), 6.67 (d, *J* = 8.28 Hz, 1H, N*H*), 4.77 (dd, *J* = 4.67/8.28 Hz, 1H, NHC*H*), 3.76 (s, 3H, OCH_3), 2.27 (m, *J* = 4.67/6.62/7.17 Hz, 1H, NHCHC*H*), 1.00 (d, *J* = 6.62 Hz, 3H, CH_3), 0.98 (d, *J* = 7.17 Hz, 3H, CH_3); $^{13}C\{^1H\}$ NMR (101 MHz, $CDCl_3$, 297 K): δ = 172.6 (*C*O), 167.3 (*C*OO), 134.1 (*i-C*), 131.7 (*p-C*H), 128.6 (*m-C*H), 127.0 (*o-C*H), 57.4 and 52.2 (NH*C*H and O*C*H_3), 31.6 (NHCH*C*H), 18.9 (*C*H_3), 17.9 (*C*H_3), IR (KBr, cm^{-1}): 3350 vs, 3075 vw, 2968 s, 2933 w, 2873 vw, 1740 vs, 1642 vs, 1521 vs, 1491 s, 1242 s, 1204 vs, 1152 s, 994 m, 751 m, 734 m, 714 m, 693 m, 629 w, 610 w, 573 w; MS (EI): *m/z* (%) = 235 $[M]^+$ (1), 176 (30), 122 (18), 105 (100), 77 (33), 51 (8), no other peaks >10%; HRMS Calc. for $C_{13}H_{17}NO_3$: 235.12085. Found: 235.12030.

5.9. Methyl 1-benzoylpyrrolidine-2-carboxylate

Colorless solid; m.p.: 81–83 °C; R_f (SiO_2, EtOAc): 0.44; ^1H NMR (400 MHz, $CDCl_3$, 297 K): δ = 7.60–7.54 (m, 2H, Ph), 7.44–7.33 (m, 2H, Ph), 4.68 (m, 1H, NC*H*), 3.78 (s, 3H, OCH_3), 3.65 (m, 1H of NCH_2), 3.55 (m, 1H of NCH_2), 2.33 (m, 1H of NCHCH_2), 2.03 (m, 2H, NCHCH_2 and NCH_2CH_2), 1.89 (m, 1H of NCH_2CH_2); $^{13}C\{^1H\}$ NMR (101 MHz, $CDCl_3$, 297 K): δ = 172.8 (*C*OO), 169.7 (*C*O), 136.2 (*i-C*), 130.2 (*p-C*H), 128.2 (*m-C*H), 127.3 (*o-C*H), 59.1 (N*C*H), 52.3 (O*C*H_3), 49.9 (N*C*H_2), 29.4 (NCH*C*H_2), 25.4 (NCH_2*C*H_2); IR (KBr, cm^{-1}): 3461 w, 2979 w, 2952 w, 2879 w, 1787 w, 1741 vs, 1624 vs, 1602 m, 1575 m, 1448 s, 1416 vs, 1356 m, 1213 s, 1198 s, 1178 s, 1041 w, 1026 w, 998 m, 799 m, 730 s, 706 m, 659 w; MS (EI) *m/z* (%) = 233 $[M]^+$ (4), 174 (39), 105 (100), 77 (34), 51 (11), no other peaks >10%; HRMS Calc. for $C_{13}H_{15}NO_3$: 233.10519. Found: 233.10540.

Acknowledgements

The authors thank S. Giertz, S. Buchholz, H. Baudisch, C. Mewes, Dr. C. Fischer, and Dr. W. Baumann for excellent technical and analytical service. Generous support of this project from DEGUSSA AG is gratefully acknowledged.

References

[1] H. Wakamatsu, J. Uda, N. Zamakami, J. Chem. Soc., Chem. Commun. (1971) 1540.
[2] (a) M. Beller, M. Eckert, Angew. Chem. 112 (2000) 1026;
Angew. Chem. Int. Ed. 39 (2000) 1010;
(b) J.F. Knifton, in: B. Cornils, W.A. Herrmann (Eds.), Applied Homogeneous Catalysis with Organometallic Compounds, VCH, Weinheim, 1996, p. 159;
(c) M. Beller, A. Jacobi von Wangelin, in: M. Beller, C. Bolm (Eds.), Transition Metals for Organic Synthesis, Wiley-VCH, Weinheim, 2004.
[3] (a) J.-J. Parnaud, G. Campari, P. Pino, J. Mol. Catal. 6 (1979) 341;
(b) P. Magnus, M. Slater, Tetrahedron Lett. 28 (1987) 2829;
(c) I. Ojima, Z. Zhang, Organometallics 9 (1990) 3122;
(d) J.J. Lin, J.K. Knifton, J. Organomet. Chem. 147 (1991) 99.
[4] (a) I. Ojima, K. Hirai, M. Fujita, K. Kato, H. Boong Kwon, I.T. Horváth, J. Am. Chem. Soc. 110 (1988) 150;
(b) I. Ojima, Chem. Rev. 88 (1988) 1011;
(c) A. Cabrera, P. Sharma, J.L. Arias, J.L. Velasco, J. Perez-Flores, R.M. Gomez, J. Mol. Catal. A 212 (2004) 19.
[5] (a) I. Ojima, K. Hirai, M. Fujita, T. Fuchikami, J. Organomet. Chem. 279 (1985) 203;
(b) I. Ojima, J. Mol. Catal. 37 (1986) 25.
[6] K. Hirai, Y. Takahashi, I. Ojima, Tetrahedron Lett. 23 (1982) 2491.
[7] J.G. de Vries, R.P. de Boer, M. Hogeweg, E.E.C.G. Gielens, J. Org. Chem. 61 (1996) 1842.
[8] (a) M. Beller, M. Eckert, F. Vollmüller, S. Bogdanovic, H. Geissler, Angew. Chem. 109 (1997) 1534;
Angew. Chem. Int. Ed. 36 (1997) 1494;
(b) G. Dyker, Angew. Chem. 109 (1997) 1777;
Angew. Chem. Int. Ed. 36 (1997) 1700;
(c) M. Beller, M. Eckert, F. Vollmüller, J. Mol. Catal. 135 (1998) 23;
(d) M. Beller, W.A. Moradi, M. Eckert, H. Neumann, Tetrahedron Lett. 40 (1999) 4523;
(e) M. Beller, M. Eckert, W. Moradi, Synlett (1999) 108;
(f) M. Beller, M. Eckert, W. Moradi, H. Neumann, Angew. Chem. 111 (1999) 1562;
Angew. Chem. Int. Ed. 38 (1999) 1454;
(g) D. Gördes, H. Neumann, A. Jacobi von Wangelin, C. Fischer, K.-H. Drauz, H.-P. Krimmer, M. Beller, Adv. Synth. Catal. 345 (2003) 510.
[9] T. Sagae, M. Sugiura, H. Hagio, S. Kobayashi, Chem. Lett. 32 (2003) 160.
[10] (a) For a discussion of the different equilibria see for example: A. Jacobi von Wangelin, H. Neumann, D. Gördes, S. Klaus, D. Strübing, M. Beller, Chem. Eur. J. 9 (2003) 4286;
(b) D. Gördes, A. Jacobi von Wangelin, S. Klaus, H. Neumann, D. Strübing, H. Jiao, W. Baumann, M. Beller, Org. Biomol. Chem. 2 (2004) 845.
[11] (a) Y. Becker, A. Eisenstadt, J.K. Stille, J. Org. Chem. 45 (1980) 2145;
(b) M.C. Cesa, J.D. Burrington, United States Patent (1987) PN 4,710,574;
(c) M.C. Cesa, J.D. Burrington, United States Patent (1988) PN 4,749,786;
(d) D.A. Freed, M.C. Kozlowski, Tetrahedron Lett. 42 (2001) 3403.
[12] R.F. Heck, D.S. Breslow, J. Am. Chem. Soc. 83 (1961) 4023.
[13] C.-F. Huo, Y.-W. Li, G.-S. Wu, M. Beller, H. Jiao, J. Phys. Chem. A 106 (2002) 12161.
[14] C.-F Huo, Y.-W. Li, M. Beller, H. Jiao, Organometallics 22 (2003) 4665.
[15] All calculations were done using the GAUSSIAN 98 program. All structures were optimized at B3LYP density functional level of theory with the LANL2DZ basis set including a set of polarizations (B3LYP/LANL2DZp) and the nature of the optimized structures on the potential energy surface was characterized by the calculated number of imaginary frequency (NImag) at the same level of theory, i.e., minimum structure without imaginary frequencies (NImag = 0), and transition state with only one imaginary frequency (NImag = 1). The frequency calculation provides zero-point energies (ZPE) and thermal correction at 298.15 K. These energetic contributions are used for the calculation of the thermodynamic properties (ΔG). Taking the entropy effect into account, our discussion is based on the free energies (ΔG) of activation and reaction, and the corresponding starting point is the most stable olefin complex (**1-CC**).
[16] C.-F. Huo, Y.-W. Li, M. Beller, H. Jiao, Organometallics 23 (2004) 2168.
[17] L. Versluis, T. Ziegler, L. Fan, Inorg. Chem. 29 (1990) 4530.
[18] S.K. Goh, D.S. Marynick, Organometallics 21 (2002) 2262.
[19] C.-F. Huo, Y.-W. Li, M. Beller, H. Jiao, Organometallics 23 (2004) 765.
[20] F.E. Hong, Y.-C. Chang, Organometallics 23 (2004) 718.